FFT solvers for transport problems in heterogeneous media

François Willot

Center for Mathematical Morphology
École des Mines, 35 rue Saint-Honoré, 77300 Fontainebleau, France.
francois.willot@ensmp.fr.

Introduction to FFT methods – Paris, March 14–18, 2022

Contents

Introduction

Scope of FFT methods

- By principle, FFT methods rely on a Green operator associated to a homogeneous material
- In mechanics, this operator serves as a projector onto the space of curl-free strain fields (small strain assumption) parallel to the space of divergence-free stress fields (quasi-static balance of linearmomentum)
- Conservation laws and field admissibility are treated in the Fourier domain whereas constitutive laws are enforced in the real space
- As such, many problems of physics involving the equivalent of the "Lippmann-Schwinger" equation can be tackled with FFT. Deriving FFT schemes is (almost) straightforward in many problems of quasi-static physics involving heterogeneous materials.

Contents

Conductivity

Linear conductivity in the continuum :

$$\partial_i J_i(\mathbf{x}) = 0, \qquad E_i(\mathbf{x}) = -\partial_i \Phi(\mathbf{x}), \qquad J_i(\mathbf{x}) = \sigma_{ij}(\mathbf{x}) E_j(\mathbf{x}),$$

where $\Phi(\mathbf{x})$ is the electric potential and $\boldsymbol{\sigma}(\mathbf{x})$ is the local conductivity tensor of the material phase at point $\mathbf{x}$.
Periodic boundary conditions are employed, in the form

$$\mathbf{J}(\mathbf{x}) \cdot \mathbf{n} - \#, \quad \Phi(\mathbf{x} + L\mathbf{e}_i) \equiv \Phi(\mathbf{x}) - \overline{E}_i L, \quad \mathbf{x}, \mathbf{x} + L\mathbf{e}_i \in \partial\Omega,$$

All FFT schemes presented in the previous talks can be deduced from the following "Lippmann-Schwinger" equation :

$$E_i = \overline{E}_i - G^0_{ij} * P_j, \quad P_j = J_j - \sigma^0 E_j,$$

Conductivity

Linear conductivity in the continuum :

$$\partial_i J_i(\mathbf{x}) = 0, \qquad E_i(\mathbf{x}) = -\partial_i \Phi(\mathbf{x}), \qquad J_i(\mathbf{x}) = \sigma_{ij}(\mathbf{x}) E_j(\mathbf{x}),$$

where $\Phi(\mathbf{x})$ is the electric potential and $\boldsymbol{\sigma}(\mathbf{x})$ is the local conductivity tensor of the material phase at point $\mathbf{x}$.
Periodic boundary conditions are employed, in the form

$$\mathbf{J}(\mathbf{x}) \cdot \mathbf{n} - \#, \quad \Phi(\mathbf{x} + L\mathbf{e}_i) \equiv \Phi(\mathbf{x}) - \overline{E}_i L, \quad \mathbf{x}, \mathbf{x} + L\mathbf{e}_i \in \partial\Omega,$$

Equivalent of the "Lippmann-Schwinger" equation in conductivity :

$$E_i = \overline{E}_i - G^0_{ij} * P_j, \quad P_j = J_j - \sigma^0 E_j,$$

Conductivity

This gives the equivalent of Moulinec & Suquet's "basic scheme" (Eyre and Milton, 1998)

$$\mathbf{E}^{(k+1)} = \overline{\mathbf{E}} - G^0 * \mathbf{P}, \quad \mathbf{P} = \mathbf{J} - \sigma^0 \mathbf{E}^{(k)},$$

with e.g. $\mathbf{E}^{(k=0)} \equiv \overline{\mathbf{E}}$.
An equivalent 'dual' formulation stems from writing the problem in terms of the electric current as

$$J_i = \overline{J}_i - H^0_{ij} * T_j, \quad T_j = E_j - \rho^0 J_j,$$

where $\rho^0 = 1/\sigma^0$ is the reference resistivity, and $\overline{\mathbf{J}}$ is the prescribed macroscopic current. The Green operator associated to the governing equation for the current reads

$$H^0_{ij}(\mathbf{x}) = \sigma^0 \left\{ [\delta(\mathbf{x}) - 1]\, \delta_{ij} - \sigma^0 G^0_{ij}(\mathbf{x}) \right\},$$

where $\delta(\mathbf{x})$ is Dirac's distribution and δ_{ij} is the Kronecker symbol. Thus, for all $\mathbf{T}$,

$$H^0_{ij} * T_j = \sigma^0 \left(T_i - \langle T_i \rangle_\Omega - \sigma^0 G^0_{ij} * T_j \right).$$

Conductivity

Remarks :

- Straightforward extension of all (or nearly all) previously-described schemes in mechanics to conductivity
- Not just algorithms, but also *all* discretization schemes can be extended to conductivity. Discretization is enforced when applying the Green operator. Symbolically :

$$\sigma_0 G^{(0)} = \frac{\text{grad}(\text{div}\cdot)}{\Delta} = \frac{\nabla^* \nabla \cdot}{\nabla^* \cdot \nabla}$$

To do so, use the representation in Fourier space for the operators ∇ and adjoint ∇^*.

Conductivity

$$\sigma_0 G^{(0)} = \frac{\mathrm{grad}(\mathrm{div}\cdot)}{\Delta} = \frac{\nabla^*\nabla\cdot}{\nabla^*\cdot\nabla}$$

Remark (i) : in linear and nonlinear conductivity, we are dealing with lower-order tensors. It is often sufficient to consider the forward-and-backward finite-difference scheme which is centered.

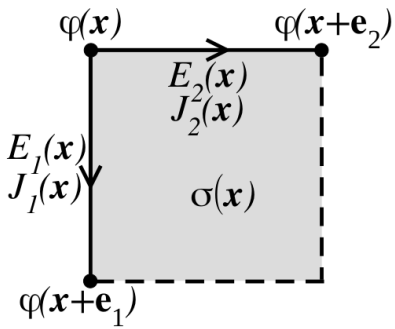

This finite-difference scheme is centered.

The "classical" discretization (all fields are trigonometric polynomials) is also possible and works fine if $\partial J(\boldsymbol{x})/\partial E(\boldsymbol{x}) > 0$.

Conductivity

$$\sigma_0 G^{(0)} = \frac{\text{grad}(\text{div}\cdot)}{\Delta} = \frac{\nabla^*\nabla\cdot}{\nabla^* \cdot \nabla}$$

Remark (ii) : when utilizing finite differences, the operators ∇ and ∇^* can be computed easily in the real space.
Fourier transforms are required, only when applying $(\nabla^* \cdot \nabla)^{-1} = \Delta^{-1}$.

$$\phi^{k+1} = \frac{1}{\sigma^0 \Delta} \mathbf{div}\left[(\sigma - \sigma^0)(\overline{\mathbf{E}} - \mathbf{grad}\phi^k)\right]$$

Provides a rewriting of the basic scheme in terms of potential (not the electric field) which is the scalar. Only one FFT (and one FFT^{-1}) is required at each step (could be more depending on the convergence criterion).

This is optimal in terms of memory (1 potential + 1 microstructure). On a 16 Gb laptop : 1560^3 voxels.

Conductivity

Remark (iii) : remark (ii) extends to mechanics, for finite-difference schemes in which strain fields are admissible at each step. For instance : staggered discretization schemes with basic gradient descent scheme.

Drawback : harder to parallelize because the computations in the real space are not local (need to provide for overlap zones).

Conductivity

Remark (iii) : remark (ii) extends to mechanics, for finite-difference schemes in which strain fields are admissible at each step. For instance : staggered discretization schemes with basic gradient descent scheme.

Drawback : harder to parallelize because the computations in the real space are not local (need to provide for overlap zones).

Conductivity

Illustration : nonlinear conductivity on a square lattice with strongly-nonlinear law.

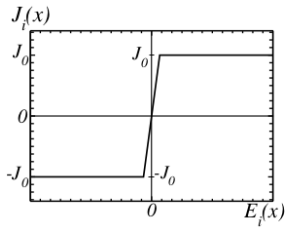

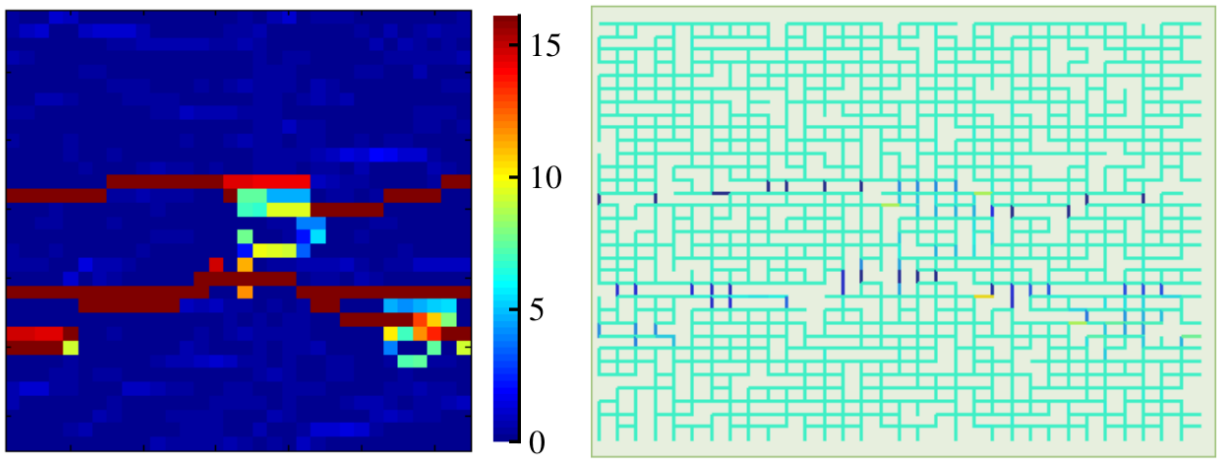

Electric field localization along minimal path. FFT computation with forward-and-backward discretization + polarization scheme (Eyre and Milton, 1998).

Perfect-plasticity

Disgression : Polarization schemes with finite-difference discretization are good at handling perfect-plasticity in mechanics in porous materials.

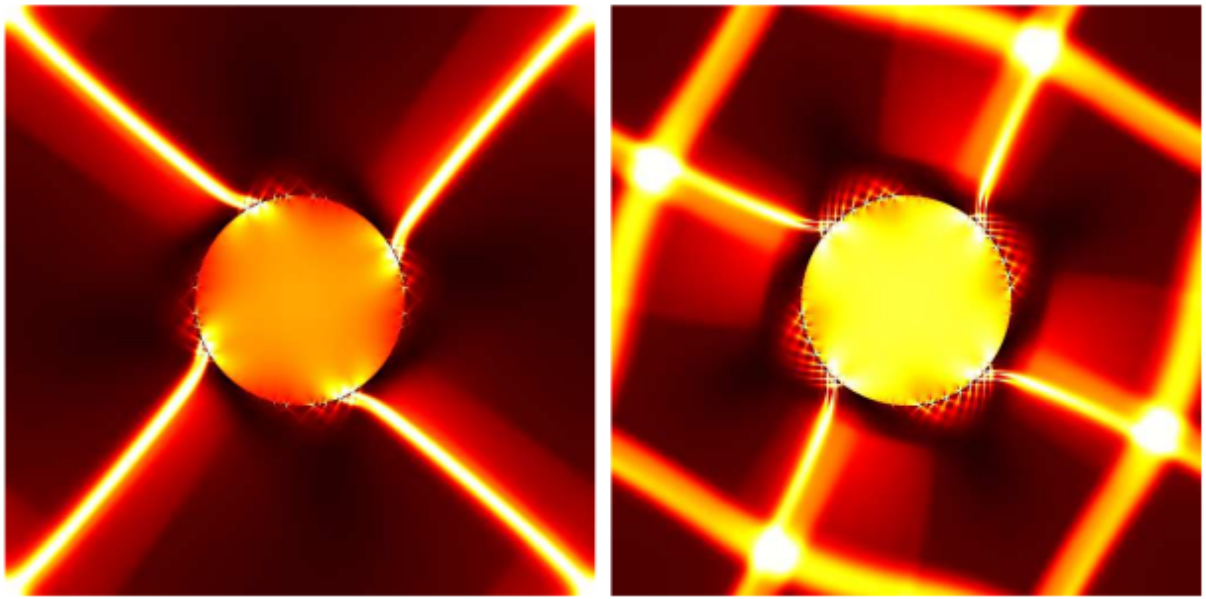

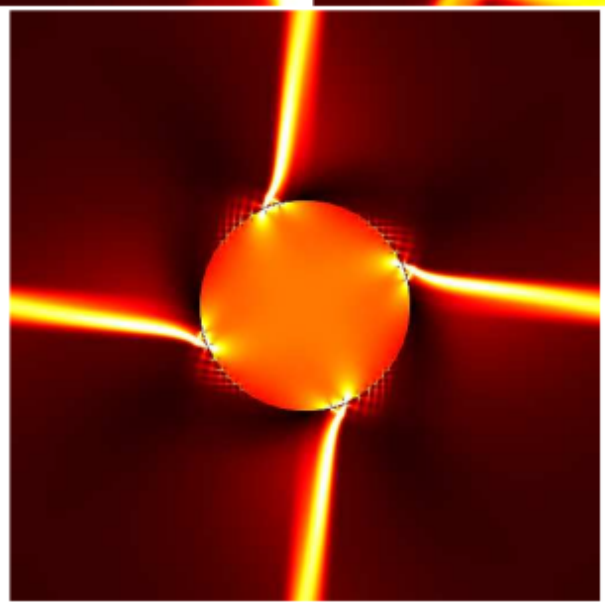

Perfect-plasticity

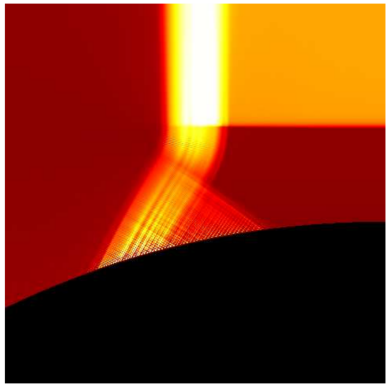
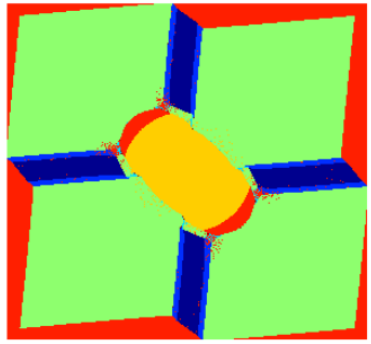
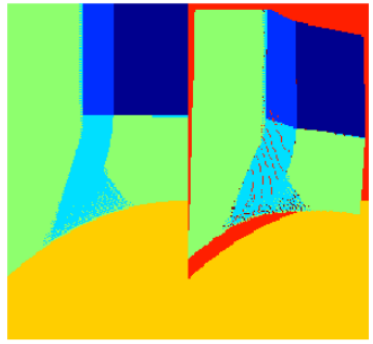

The periodic part of the displacement is computed from the strain field as (Gasnier et al, 2018) :

$$|\boldsymbol{k}|^4 u_1 = \left(2|\boldsymbol{k}|^2 - |k_1|^2\right) k_1^* \varepsilon_{11} - k_1 \left[\left(k_2^*\right)^2 \varepsilon_{22} + \left(k_3^*\right)^2 \varepsilon_{33}\right] + 2\left(|\boldsymbol{k}|^2 - |k_1|^2\right)\left[k_2^* \varepsilon_{12} + k_3^* \varepsilon_{13}\right] - 2k_1 k_2^* k_3^* \varepsilon_{23}$$

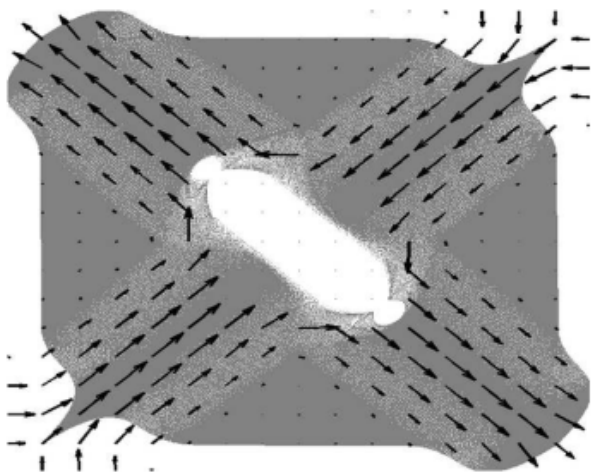
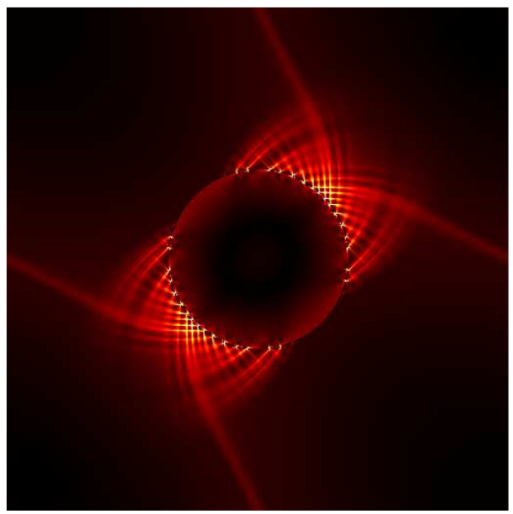
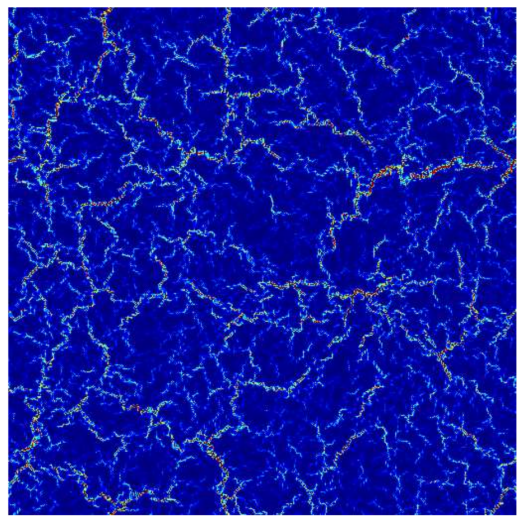

Conductivity

Remark (iv) this scheme solves all "diffusion" problems with many mathematically – albeit not physically – identical equations, equivalent to the first and second Fick law in static.

Heat conduction (Fourier's law) : $\mathbf{J}(\mathbf{x}) = k\text{grad}\,T(\mathbf{x})$

- $T(\mathbf{x})$ [T] : temperature at point $\mathbf{x}$
- $\mathbf{J}(\mathbf{x})$ [W/m^2] : local heat flux
- k [W/m/K] : thermal conductivity
- Steady-state (constant temperature gradient) : $\text{div}\mathbf{J}(\mathbf{x}) = 0$

Magnetic permeability : $\mathbf{B}(\mathbf{x}) = \mu(\mathbf{x})\mathbf{H}(\mathbf{x})$
First Maxwell equation : $\text{rot}\mathbf{H} = 0$ or $\mathbf{H} = -\text{grad}\,U$

- $\mathbf{B}(\mathbf{x})$ [T] : magnetic field at point $\mathbf{x}$
- $\mathbf{H}(\mathbf{x})$ [TA^2/N] : auxiliary magnetic field
- μ [N/A^2] : magnetic permeability
- U : magnetic potential
- Gauss's law : $\text{div}\mathbf{B}(\mathbf{x}) = 0$

Conductivity

Darcy's law : $\mathbf{q}(\mathbf{x}) = \frac{-k}{\mu} \text{grad} P(\mathbf{x})$

- $P(\mathbf{x})$ [N/m^2] : pressure at point $\mathbf{x}$
- $\mathbf{q}(\mathbf{x})$ [(m^3/(m^{2}s)] : fluid flow
- k [m^2] : permeability
- μ [Pa s] fluid viscosity

Hydrogeology, gaz diffusion.

Dielectric permittivity : $\mathbf{D}(\mathbf{x}) = \varepsilon \mathbf{E}(\mathbf{x})$

- ε [F/m] : absolute permittivity
- $\mathbf{D}(\mathbf{x})$ [C/m^2] : electric displacement field at point $\mathbf{x}$
- $\mathbf{E}(\mathbf{x})$ [N/C] : electric field

Conductivity

Coupling. Piezoelectricity (Brenner et al, Phys Rev. B 2009).

$$\boldsymbol{\varepsilon}(\boldsymbol{x}) = \overline{\boldsymbol{\varepsilon}} - \boldsymbol{\Gamma}^0 * \boldsymbol{\tau}(\boldsymbol{x}) - {}^{\mathrm{T}}\boldsymbol{\Upsilon}^0 * \boldsymbol{P}(\boldsymbol{x}), \quad \forall\, \boldsymbol{x} \in \Omega,$$

$$\boldsymbol{E}(\boldsymbol{x}) = \overline{\boldsymbol{E}} + \boldsymbol{\Upsilon}^0 * \boldsymbol{\tau}(\boldsymbol{x}) + \boldsymbol{\Delta}^0 * \boldsymbol{P}(\boldsymbol{x}), \quad \forall\, \boldsymbol{x} \in \Omega,$$

NB : imperfect interfaces are much more difficult to handle. Schemes developed by Monchiet for Kapitza interfaces (2018).

Wicht et al (2020) : thermechanical coupling.

Contents

Electrostatics

Extension to quasi-optics with time-harmonic solicitations. All fields are proportional to $\mathbf{e}^{i\omega t}$ where ω is the frequency of the sollicitation.

Maxwell equations : $\mathrm{rot}[\mathrm{rot}\mathbf{E}(\mathbf{x})] = \omega^2 \mathbf{D}(\mathbf{x})$

Quasi-static assumption $\omega \ll \delta$: $\mathrm{rot}\mathbf{E} = 0$ or $\mathbf{E} = -\mathrm{grad}\, U$

$\mathrm{div}\boldsymbol{D}(\boldsymbol{x}) \equiv 0$ also in electrodynamics.

Optical properties at wavelengths small compared to the typical size of the material.

Green operator :

$$G_{ij}^{(0)} = \frac{1}{\sigma_0} \frac{k_i k_j^*}{k_i k_i^*}.$$

In a way, the implementation becomes even easier as complex-to-complex Fourier transforms are required.

Electrostatics

Prediction of optical properties of a hematite coating, with nanoparticles.

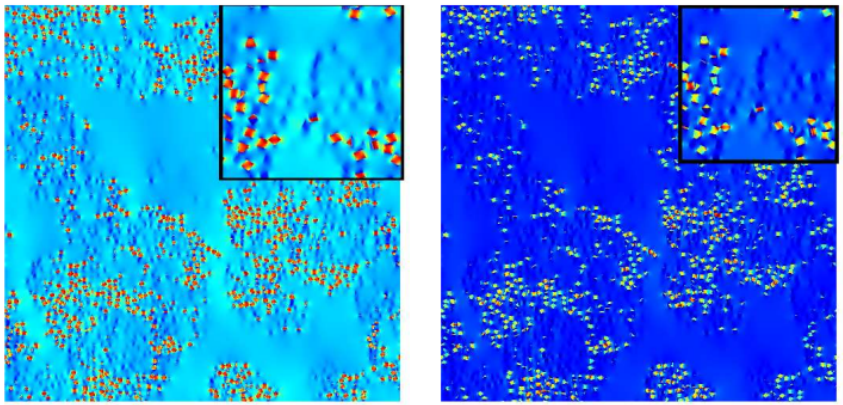

(a) $\mathrm{Re}(D_1)$, $\lambda = 401\mathrm{nm}$ (b) $\mathrm{Im}(D_1)$, $\lambda = 401\mathrm{nm}$

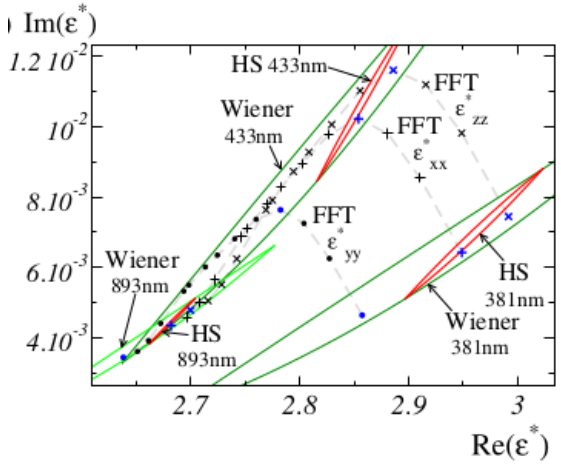

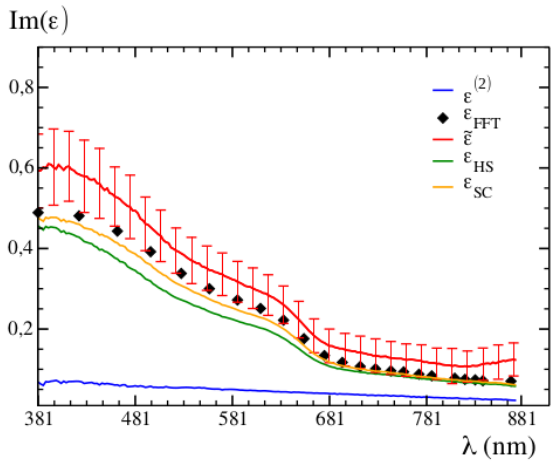

(Couka et al, Adv. Sc. Med. and Engng, 2014 ; Azzimonti et al, J. of Modern Optics, 2014)

Contents

Viscoelasticity with Prony series

Time-harmonic regime in mechanics ?

- *Fourier decomposition in time :* strain and stress history specified as a series of harmonics. *Complex elastic moduli*
- *Fourier decomposition in space :* use of a Green operator associated to the solution for a homogeneous elastic stiffness tensor
- Discretization of complex microstructures on a regular grid of voxels ; periodic boundary conditions
- Full-fields reconstruction in space and time

Problem setup

Time-harmonic sollicitation

$$\widetilde{\boldsymbol{\varepsilon}}(\boldsymbol{x};t)=\boldsymbol{\varepsilon}(\boldsymbol{x})\mathbf{e}^{\mathbf{i}\omega t},\qquad \widetilde{\boldsymbol{\sigma}}(\boldsymbol{x};t)=\boldsymbol{\sigma}(\boldsymbol{x})\mathbf{e}^{\mathbf{i}\omega t},\qquad \widetilde{\boldsymbol{u}}(\boldsymbol{x};t)=\boldsymbol{u}(\boldsymbol{x})\mathbf{e}^{\mathbf{i}\omega t}\quad(1)$$

N.B. physical fields

$$\widehat{\boldsymbol{\varepsilon}}(\boldsymbol{x};t)=\mathbf{Re}\left[\widetilde{\boldsymbol{\varepsilon}}(\boldsymbol{x};t)\right],\quad \widehat{\boldsymbol{\sigma}}(\boldsymbol{x};t)=\mathbf{Re}\left[\widetilde{\boldsymbol{\sigma}}(\boldsymbol{x};t)\right],\quad \widehat{\boldsymbol{u}}(\boldsymbol{x};t)=\mathbf{Re}\left[\widetilde{\boldsymbol{u}}(\boldsymbol{x};t)\right]$$

Small deformation, steady-state regime

$$\widetilde{\varepsilon}_{ij}(\boldsymbol{x};t)=\frac{1}{2}\left[\partial_j\widetilde{u}_i(\boldsymbol{x};t)+\partial_i\widetilde{u}_j(\boldsymbol{x};t)\right],\qquad \partial_i\widetilde{\sigma}_{ij}(\boldsymbol{x};t)=0.$$

$$\varepsilon_{ij}(\boldsymbol{x};t)=\frac{1}{2}\left[\partial_j u_i(\boldsymbol{x};t)+\partial_i u_j(\boldsymbol{x};t)\right],\qquad \partial_i\sigma_{ij}(\boldsymbol{x};t)=0.$$

Local response

Linear-elastic inclusions :

$$\widetilde{\boldsymbol{\sigma}}(\boldsymbol{x};t) = \mathbb{C}_2 : \widetilde{\boldsymbol{\varepsilon}}(\boldsymbol{x};t), \qquad \boldsymbol{\sigma}(\boldsymbol{x}) = \mathbb{C}_2 : \boldsymbol{\varepsilon}(\boldsymbol{x}),$$

Visco-elastic matrix :

$$\widetilde{\boldsymbol{\sigma}}(\boldsymbol{x};t) = \int_{-\infty}^{t} \mathrm{d}\tau\, \mathbb{C}_1(t-\tau) : \frac{\mathrm{d}\widetilde{\boldsymbol{\varepsilon}}(\boldsymbol{x};\tau)}{\mathrm{d}\tau}.$$

For an isotropic tensor $\mathbb{C}_1$:

$$\boldsymbol{\sigma}(\boldsymbol{x}) = \mathbb{C}_1^*(\kappa_1^*, \mu_1^*) : \boldsymbol{\varepsilon}(\boldsymbol{x})$$

with :

$$\kappa_1^*(\mathbf{i}\omega) = \overline{\kappa_1} + \mathbf{i}\omega \int_0^\infty \mathrm{d}\eta\, \left[\kappa_1(\eta) - \overline{\kappa_1}\right] \mathbf{e}^{-\mathbf{i}\omega\eta},$$

$$\mu_1^*(\mathbf{i}\omega) = \overline{\mu_1} + \mathbf{i}\omega \int_0^\infty \mathrm{d}\eta\, \left[\mu_1(\eta) - \overline{\mu_1}\right] \mathbf{e}^{-\mathbf{i}\omega\eta},$$

$$\overline{\kappa_1} = \lim_{t\to\infty} \kappa_1(t) \geqslant 0, \qquad \overline{\mu_1} = \lim_{t\to\infty} \mu_1(t) \geqslant 0.$$

Local response

Example (Maxwell model) :

$$\frac{\widetilde{\sigma}'(t)\mathrm{d}t}{t_1} + \mathrm{d}\widetilde{\sigma}'(t) = 2\mu_0 \mathrm{d}\widetilde{\varepsilon}'(t), \quad \frac{\widetilde{\sigma}_{kk}(t)\mathrm{d}t}{t_1} + \mathrm{d}\widetilde{\sigma}_{kk}(t) = 3\kappa_0 \mathrm{d}\widetilde{\varepsilon}_{kk}(t)$$

This is equivalent to (Christensen, 2012) :

$$\widetilde{\sigma}'(t) = \int_{-\infty}^{t} \mathrm{d}\tau \, 2\mu_1(t-\tau)\frac{\mathrm{d}\widetilde{\varepsilon}'(\tau)}{\mathrm{d}\tau}, \quad \widetilde{\sigma}_{kk}(t) = \int_{-\infty}^{t} \mathrm{d}\tau \, 3\kappa_1(t-\tau)\frac{\mathrm{d}\widetilde{\varepsilon}_{kk}(\tau)}{\mathrm{d}\tau},$$

with

$$\mu_1(t) = \mu_0 \mathbf{e}^{-t/t_1}\mathcal{H}(t), \qquad \kappa_1(t) = \kappa_0 \mathbf{e}^{-t/t_1}\mathcal{H}(t), \qquad \mathcal{H}(t) = \begin{cases} 0 & \text{if } t < 0, \\ 1 & \text{if } t > 0. \end{cases}$$

Time-FFT provides the complex moduli :

$$\mu_1^*(\mathbf{i}\omega) = \frac{\mu_0}{1 + 1/(\mathbf{i}\omega t_1)}, \quad \kappa_1^*(\mathbf{i}\omega) = \frac{\kappa_0}{1 + 1/(\mathbf{i}\omega t_1)}.$$

Boundary conditions

Periodic boundary conditions with time-harmonic macroscopic strain loading

$$\langle \boldsymbol{\varepsilon}(\boldsymbol{x}) \rangle = \overline{\boldsymbol{\varepsilon}}, \quad \boldsymbol{\varepsilon}(\boldsymbol{x})\,\#, \quad \boldsymbol{\sigma}(\boldsymbol{x})\,\#.$$

Effective properties

$$\overline{\boldsymbol{\sigma}} = \langle \boldsymbol{\sigma}(\boldsymbol{x}) \rangle = \mathbb{C}^{\mathsf{eff}} : \overline{\boldsymbol{\varepsilon}}.$$

N.B. for non-harmonic strain loading $\alpha(t) = \langle \widetilde{\boldsymbol{\varepsilon}}(\boldsymbol{x}; t) \rangle$

$$\alpha(t) = \frac{1}{2\pi} \int_{-\infty}^{\infty} \mathrm{d}\omega\, \alpha(\omega) \mathbf{e}^{\mathbf{i}\omega t}.$$

Strain field recovered as a superposition of harmonic responses

$$\widetilde{\boldsymbol{\varepsilon}}(\boldsymbol{x}; t) = \frac{1}{2\pi} \int_{-\infty}^{\infty} \mathrm{d}\omega\, \boldsymbol{\varepsilon}_{\omega}(\boldsymbol{x}) \mathbf{e}^{\mathbf{i}\omega t}.$$

FFT scheme for the viscoelastic response

Extension of FFT scheme to complex elastic moduli straightforward but differ in one instance. Symmetry with complex-valued fields :

$$\widehat{\varepsilon}_{kl}(\boldsymbol{x};t) = \widehat{\varepsilon}_{lk}(\boldsymbol{x};t), \quad \widehat{\boldsymbol{\sigma}}_{kl}(\boldsymbol{x};t) = \widehat{\boldsymbol{\sigma}}_{lk}(\boldsymbol{x};t),$$

$$\varepsilon_{kl}(\boldsymbol{x}) = \varepsilon_{lk}(\boldsymbol{x}), \quad \boldsymbol{\sigma}_{kl}(\boldsymbol{x}) = \boldsymbol{\sigma}_{lk}(\boldsymbol{x}).$$

$$G^0_{ij,kl}(\mathbf{q}) = G^0_{ji,kl}(\mathbf{q}) = G^0_{ij,lk}(\mathbf{q}) = \left[G^0_{kl,ij}(\mathbf{q})\right]^* .$$

$$C^0_{ij,kl} = C^0_{ji,kl} = C^0_{ij,lk} = \left(C^0_{kl,ij}\right)^* = C^0_{kl,ij},$$

The reference must be real. Scheme applied with basic scheme (Figliuzzi et al, 2016) or polarization-based method (Gallican et al, 2019 ; André et al, 2021). They use : $\kappa_0 = \sqrt{\kappa_1 \kappa_2}$, $\mu_0 = \sqrt{\mu_1 \mu_2}$.

Validation : FE-FFT comparison

Stiff inclusion with periodic boundary conditions embedded in a viscoelastic matrix defined by a Prony series. Local stress $\sigma_m(\boldsymbol{x})$ (2D section). FEM (Abaqus) vs. FFT.

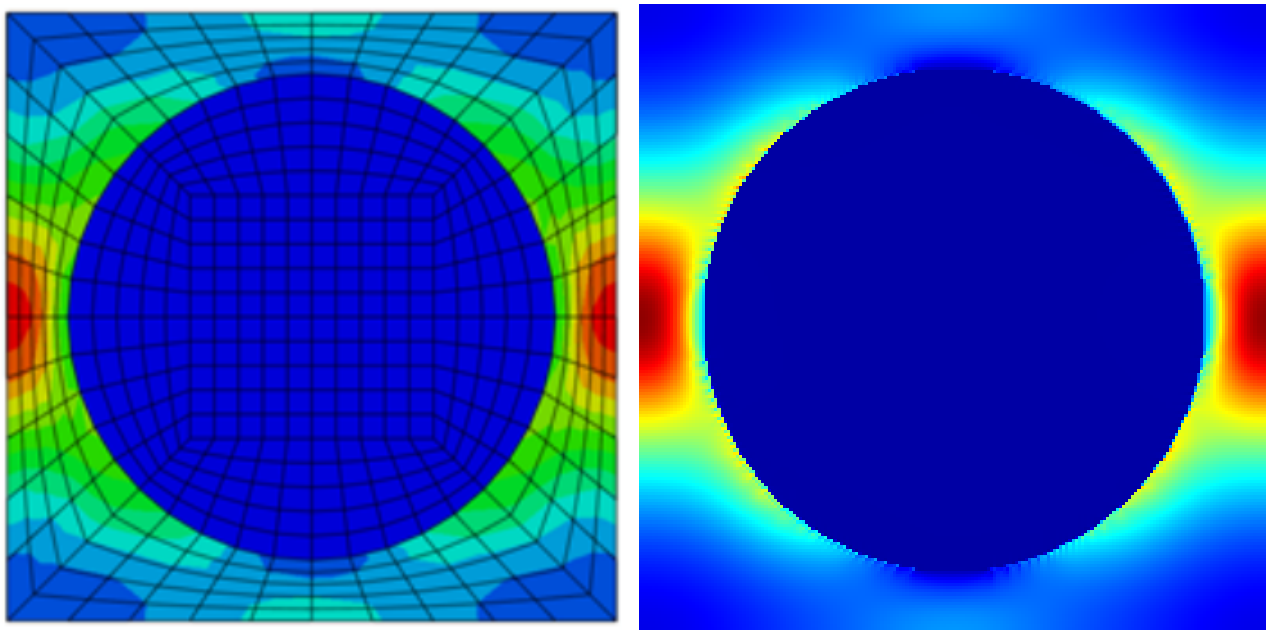

From Figliuzzi et al, 2016.

Validation : comparison with analytical estimates

Loss angle $\delta = \mathcal{I}\left(\mu^{\text{eff}}\right)/\mathcal{R}\left(\mu^{\text{eff}}\right)$, periodic array of spheres of radius R
Viscoelastic matrix defined by a Prony series.

f (Hz)	$R = 0$		$R = 5$	
	Cohen (2004)	FFT	Cohen (2004)	FFT
1	0.033504	0.033504	0.033504	0.033502
5	0.038662	0.038662	0.038661	0.038659
10	0.040469	0.040469	0.040468	0.040466
50	0.04646	0.04646	0.04646	0.046456
100	0.050326	0.050326	0.050325	0.050322
	$R = 20$		$R = 40$	
1	0.033479	0.033451	0.033054	0.032757
5	0.038631	0.038598	0.038123	0.037769
10	0.040436	0.040401	0.039895	0.039519
50	0.046421	0.04638	0.045773	0.045326
100	0.050282	0.050237	0.049567	0.049074

FFT maps

Silica and carbon black materials used as nanoscopic fillers to improve the stiffness of rubbers (from Figliuzzi et al.).
Mean stress field $\mathbf{Im}(\sigma_{xy})$ (2D section). Material subjected to strain loading $\varepsilon_{xy} = 1\%$. Frequency : $\omega = 1117$ Hz.

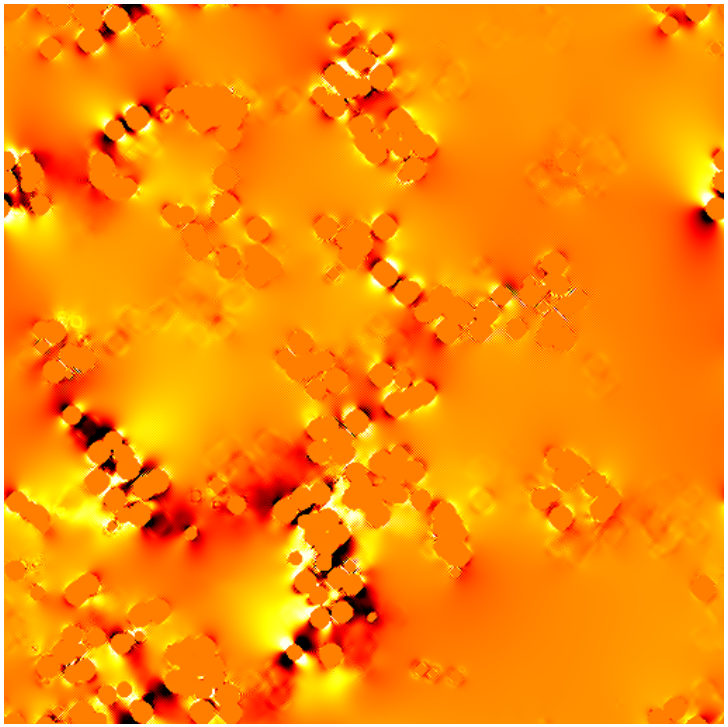

512^3 voxel grids (Figliuzzi et al, 2016)

Effective response

Effective shear modulus μ^{eff} vs. frequency ω

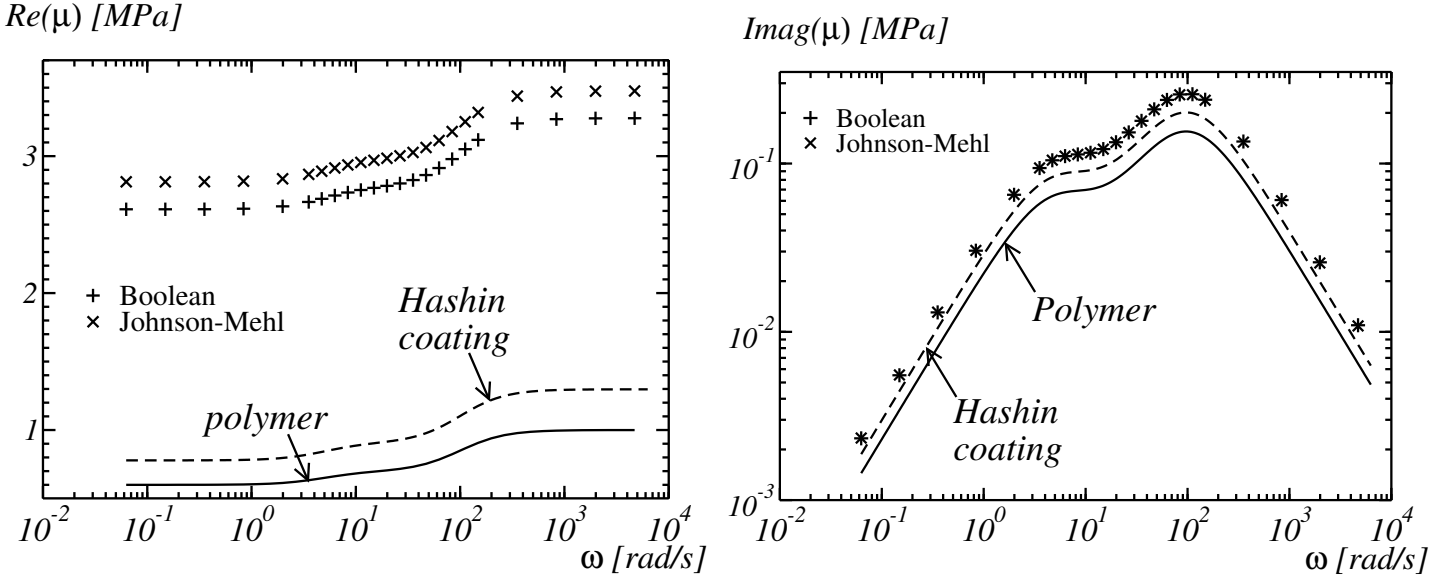

Rigorous bounds on the complex shear and bulk moduli of two-phase media given by Milton & Berryman (1997)

Viscoelasticity

Comparison with a time-explicit scheme :

$$\frac{\widetilde{\sigma'}(t)\mathrm{d}t}{t_1} + \mathrm{d}\widetilde{\sigma'}(t) = 2\mu_0 \mathrm{d}\widetilde{\varepsilon'}(t), \quad \frac{\widetilde{\sigma}_{kk}(t)\mathrm{d}t}{t_1} + \mathrm{d}\widetilde{\sigma}_{kk}(t) = 3\kappa_0 \mathrm{d}\widetilde{\varepsilon}_{kk}(t)$$

$$\widehat{\varepsilon}(\mathbf{x}; t) = 0, \qquad \widehat{\sigma}(\mathbf{x}; t) = 0$$

for $t < t_0$. For $t \geqslant t_0$, the material is subject to harmonic strain loading :

$$\langle \widehat{\varepsilon}(\mathbf{x}; t) \rangle = \cos(\omega t)\overline{\varepsilon}$$

Take $t_0 = \pi/(2\omega)$. The stress field σ at time $t + \mathrm{d}t$ is then computed by explicit time-discretization. For instance, for the deviatoric parts :

$$\Delta\widehat{\sigma}\prime(\mathbf{x}, t) = 2\mu^0 \Delta\widehat{\varepsilon}\prime(\mathbf{x}, t) - \frac{\widehat{\sigma}\prime(\mathbf{x}, t)\Delta t}{t_1},$$

$$\Delta\widehat{\sigma}\prime(\mathbf{x}, t) = \widehat{\sigma}\prime(\mathbf{x}, t + \Delta t) - \widehat{\sigma}\prime(\mathbf{x}, t), \quad \Delta\widehat{\varepsilon}\prime(\mathbf{x}, t) = \widehat{\varepsilon}\prime(\mathbf{x}, t + \Delta t) - \widehat{\varepsilon}\prime(\mathbf{x}, t).$$

Equivalent to a thermoelastic stress-strain relation with unknown $\Delta\widehat{\varepsilon}$ and $\Delta\widehat{\sigma}$ and with applied strain loading :

$$\langle \Delta\widehat{\varepsilon}\prime(\mathbf{x}, t) \rangle = -\omega \sin(\omega t)\Delta t\overline{\varepsilon}$$

See e.g. Badulescu et al (2015).

Viscoelasticity

Example (stiff inclusion in Maxwell matrix, periodic array of spheres, from Figliuzzi et al.)

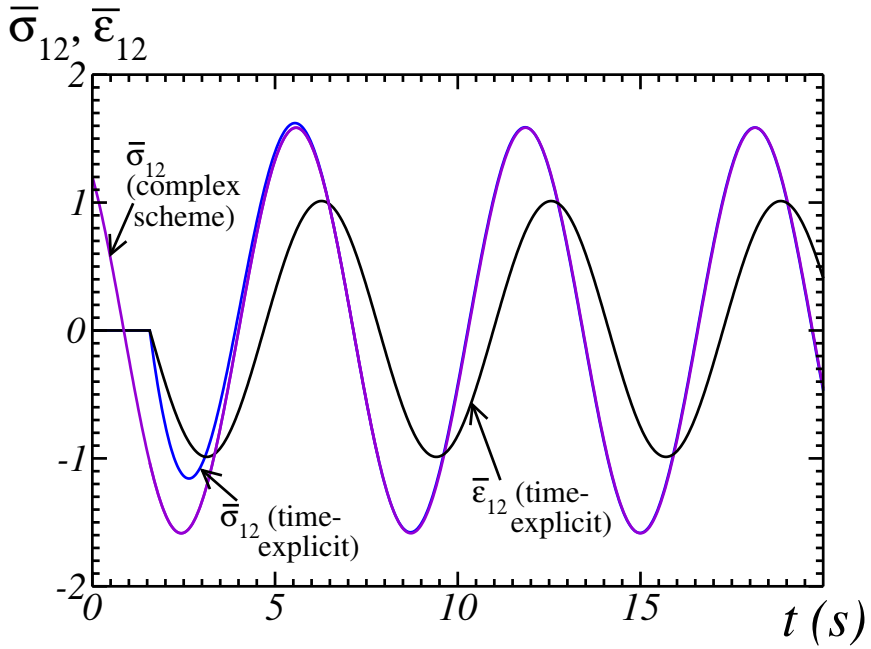

Pros and cons : the Prony series FFT scheme is useful for complex viscoelastic laws that require a large number of fields at previous time steps. In the harmonic case, the memory required is only two times that of the classical "real" schemes. Cons : harmonic regimes only ; must be linear viscoelasticity.

Contents

Damage in heterogeneous media

Polycrystal subjected to thermal cycles (cooling, re-heating)

Describe damage evolution : initiation, propagation. Strongly nonlinear problem. Irreversibility.

Variational principle

Total energy of a domain Ω containing cracks along surfaces Γ, submitted to a deformation field $\varepsilon(\boldsymbol{x})$.

$$E(\varepsilon, \Gamma) = E(\varepsilon) + E(\Gamma) = \int_{\Omega \setminus \Gamma} W(\varepsilon(\boldsymbol{x}))\mathrm{d}\boldsymbol{x} + \gamma_c \int_{\Gamma} \mathrm{d}S$$

$E(\varepsilon)$: stored elastic energy ; $E(\Gamma)$ fracture surface energy, according to Griffith criterion of fracture ; γ_c thoughness (specific surface energy).
Variational principle of Francfort and Marigo (JMPS, 1998). The total energy (over all admissible fields ε) is minimized during the fracture process :

$$(\boldsymbol{\varepsilon}, \Gamma) = \mathrm{arginf}_{(\boldsymbol{\varepsilon}, \Gamma)} \left\{ \int_{\Omega \setminus \Gamma} \frac{1}{2} \boldsymbol{\varepsilon}(\boldsymbol{x}) : \mathbb{C}(\boldsymbol{x}) : \boldsymbol{\varepsilon}(\boldsymbol{x}) + \gamma_c \int_{\Gamma} \mathrm{d}S \right\}$$

in elasticity.

Variational principle

Solve :

$$(\boldsymbol{\varepsilon}, \Gamma) = \text{arginf}_{(\boldsymbol{\varepsilon},\Gamma)} \left\{ \int_{\Omega\setminus\Gamma} \frac{1}{2}\boldsymbol{\varepsilon}(\boldsymbol{x}) : \mathbb{C}(\boldsymbol{x}) : \boldsymbol{\varepsilon}(\boldsymbol{x}) + \gamma_c \int_\Gamma \mathrm{d}S \right\}$$

in the space of physically-admissible strain fields :

$$\boldsymbol{\varepsilon} \in \mathcal{K}(\overline{\boldsymbol{\varepsilon}}) = \{\boldsymbol{\varepsilon}; \exists \boldsymbol{u} : \ \boldsymbol{\varepsilon} = (\nabla \boldsymbol{u})_{\text{sym}}, \ \langle \boldsymbol{\varepsilon} \rangle = \overline{\boldsymbol{\varepsilon}}\}$$

(assuming small deformations). At fixed Γ (no damage evolution) : the stress tensor $\boldsymbol{\sigma} = \mathbb{C} : \boldsymbol{\varepsilon}$ is divergence-free ($\text{div}\boldsymbol{\sigma} = 0$, $\boldsymbol{\sigma} \cdot \boldsymbol{n}$ is the force per unit surface)

NB : Mumford-Shah functional :

$$\min_{(u,\Gamma)} \left\{ \int_{\Omega\setminus\Gamma} |u - g|^2 + \gamma_c \int_\Gamma \mathrm{d}S + \int_{\Omega\setminus\Gamma} |\nabla u|^2 \right\}$$

Variational principle

One-dimensional problem : beam under traction (Bourdin, 2007)

Before fracture, at the onset of fracture, after failure

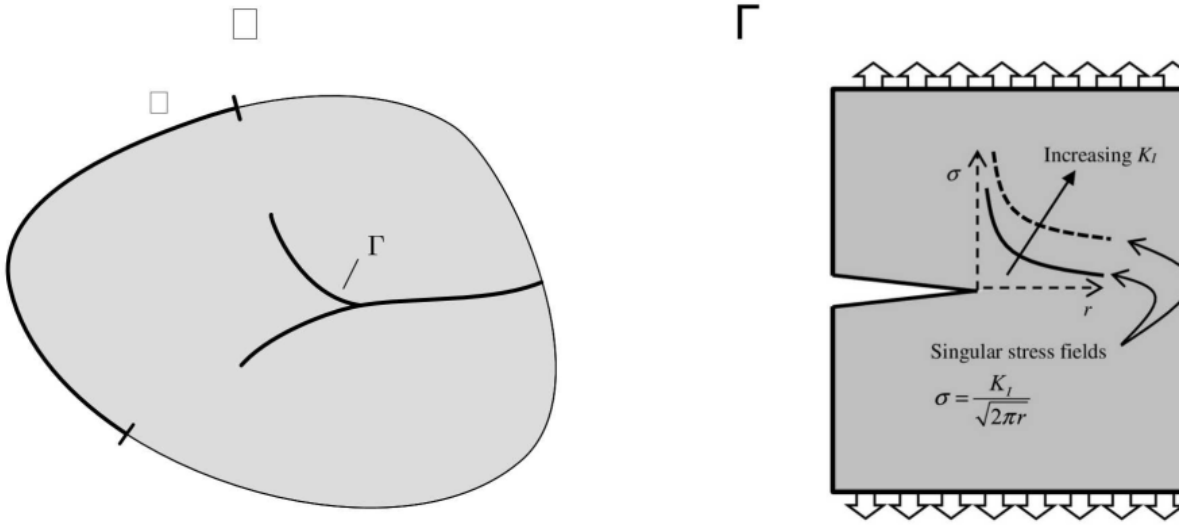

Phase field models for fracture of homogeneous isotropic media

The variational principle can not in general be solved numerically.

Regularization : introduction of a phase field $\Phi(\boldsymbol{x})(0 \leqslant \Phi(\boldsymbol{x}) \leqslant 1)$ with $\Phi(\boldsymbol{x}) \equiv 1$ along the crack and $\Phi(\boldsymbol{x}) = 0$ away from the crack. This setting requires an additional length scale parameter ℓ.
The volume integral $E(\varepsilon)$ is replaced by $\int_\Omega (1-\Phi)^2 W(\varepsilon(\boldsymbol{x}))\mathrm{d}x$.

The surface integral $E(\Gamma)$ is replaced by $\gamma_c \int_\Omega (\frac{1}{2\ell}\Phi^2 + \frac{\ell}{2}\nabla\Phi\cdot\nabla\Phi)\mathrm{d}x$ (Bourdin, 2007 ; Bourdin, Francfort and Marigo, 2008).

Resulting variational principle : minimization over admissible stress field and $\Phi(\boldsymbol{x})$ of the volume integrals

$$\text{arginf}_{(\varepsilon,\Phi)} \left\{ \int_\Omega (1-\Phi)^2 W(\varepsilon(\boldsymbol{x}))\mathrm{d}\boldsymbol{x} + \gamma_c \int_\Omega \mathrm{d}x \left(\frac{1}{2\ell}\Phi^2 + \frac{\ell}{2}\nabla\Phi\cdot\nabla\Phi \right) \right\}$$

$$\boldsymbol{\varepsilon} \in \mathcal{K}(\overline{\boldsymbol{\varepsilon}}) = \{\boldsymbol{\varepsilon}; \exists \boldsymbol{u} : \ \boldsymbol{\varepsilon} = (\nabla \boldsymbol{u})_{\text{sym}}, \ \langle \boldsymbol{\varepsilon} \rangle = \overline{\boldsymbol{\varepsilon}}\}$$

Enough to do initiation and propagation.

Phase field models for fracture of homogeneous isotropic media

Usually solved by Finite Element Methods.
From Kalthoff and Winkler (1987) (left) and Hokacker (2012) (right).

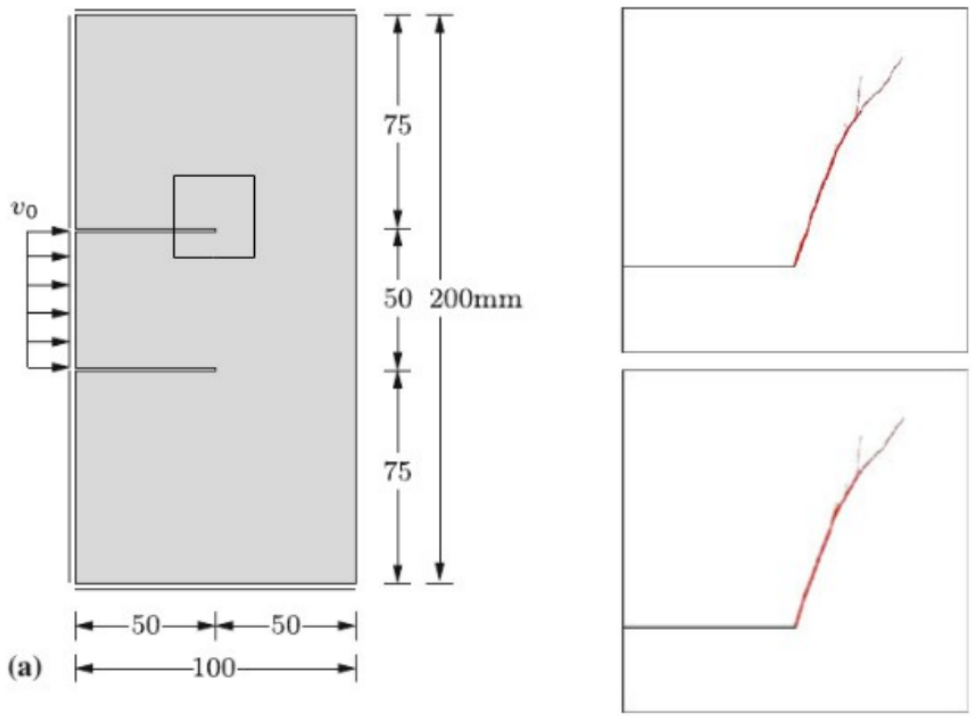

PDE for the phase field model

Functional minimization provides :

$$\varepsilon(\boldsymbol{x}) = (\nabla \boldsymbol{u}(\boldsymbol{x}))_{\text{sym}}, \qquad \langle \varepsilon(\boldsymbol{x}) \rangle = \overline{\varepsilon},$$
$$\boldsymbol{\sigma} = (1-\phi(\boldsymbol{x}))^2 \mathbb{C}(\boldsymbol{x}) : \varepsilon(\boldsymbol{x}), \qquad \text{div}(\boldsymbol{\sigma}) = 0.$$

for the linear elastic problem.

For the phase-field problem (Miehe, IJNME 2010) :

$$2(1-\Phi)\mathcal{H} - \gamma_c/\ell(\Phi - \ell^2 \Delta \Phi) = 0$$

with elastic energy $\mathcal{H}(\boldsymbol{x}, t) = W(\varepsilon) = \frac{1}{2}\varepsilon : \mathbb{C} : \varepsilon$ acting as "source term".

Irreversibility : $\mathcal{H}(\boldsymbol{x}, t) = \sup_{\tau < t} W(\varepsilon, \tau)$

Fourier-based method

Unilateral law. Essential in compression. E.g. model of Miehe :
$\sigma = (1-\phi)^2\mathbb{C} : \boldsymbol{\varepsilon}^+\mathbb{C} : \boldsymbol{\varepsilon}^-$, $\boldsymbol{\varepsilon}^{\pm} = \varepsilon_k^{\pm} n_k \oplus n_k$.

Irreversibility. ϕ can not decrease. Change the source term :
$\mathcal{H}(\boldsymbol{x}, t) = \max_{0 \leqslant s \leqslant t} \{\Psi^+(x, s)\}$ with $\Psi^+(\varepsilon) = \Psi^+(\varepsilon^+)$ (depends on the tensile parts of the strain due to unilateral effect).

Anisotropic tenacity (second-order tensor).

Non-zero elastic moduli in regions where $\phi = 1$ using :
$(1-\phi(\boldsymbol{x}))^2\mathbb{C}(\boldsymbol{x}) \rightarrow (1-\phi(\boldsymbol{x})+k)^2\mathbb{C}(\boldsymbol{x})$ with $k << 1$
Damping parameter :

$$2(1-\Phi)\mathcal{H} - \gamma_c/\ell(\Phi - \ell^2\Delta\Phi) = \eta\dot{\phi}$$

Fourier-based method

Chen and Gelebart (2021) proposed to solve the equation in ϕ with a "basic scheme"

$$\phi^{(k+1)}(\boldsymbol{q}) = \frac{\chi^k(\boldsymbol{q})}{A_0 + \boldsymbol{q}\cdot\boldsymbol{q}}, \qquad \chi^k(\boldsymbol{x} = B(\boldsymbol{x}) - (A(\boldsymbol{x} - A_0)\phi(\boldsymbol{x}),$$

(terms A_0 and B detailed in Chen and Gélébart, 2021). χ is the polarization field for phase-field problem and we use the Green operator associated to the Helmholtz equation (no pole).

Several strategies are possible (not detailed here) :
"sequential" : solve each problem for ε and ϕ separately (small time steps required). Each problem in ε and ϕ is convex.
"implicit" : solve the full problem at each time step.
Other authors proposed FFT methods for phase field problem, e.g. Jeulin (IJSS, 2021) or Ernesti et al (2021) who used an implicit solver.

Phase field models for fracture of homogeneous isotropic media

Phase-field predicted by Chen and Gélébart (2021)

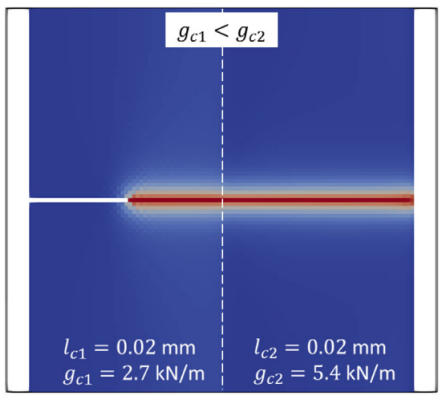

(f)

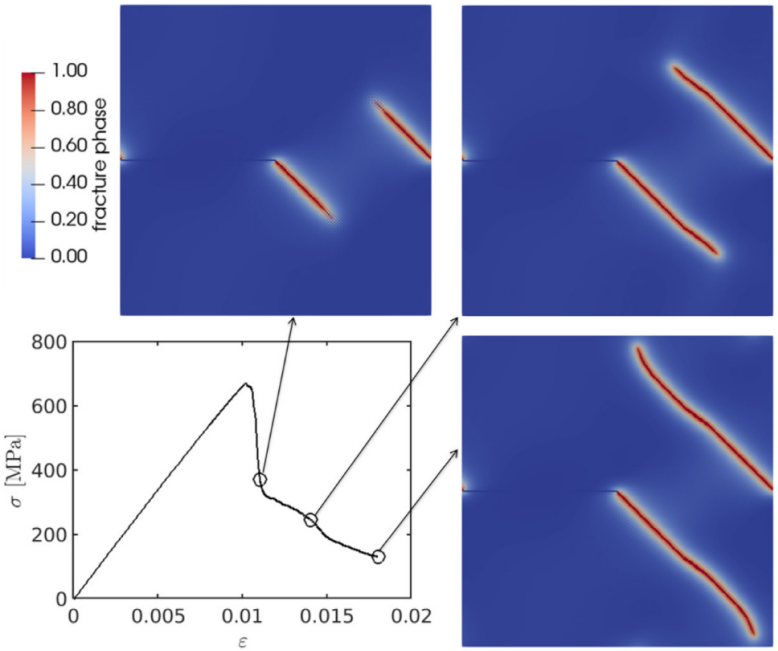

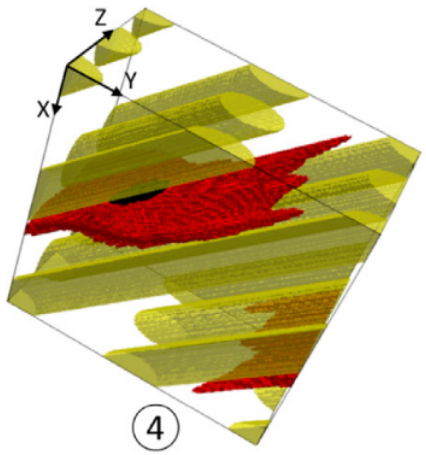

Phase field models for fracture of homogeneous isotropic media

Comparison with finite element method

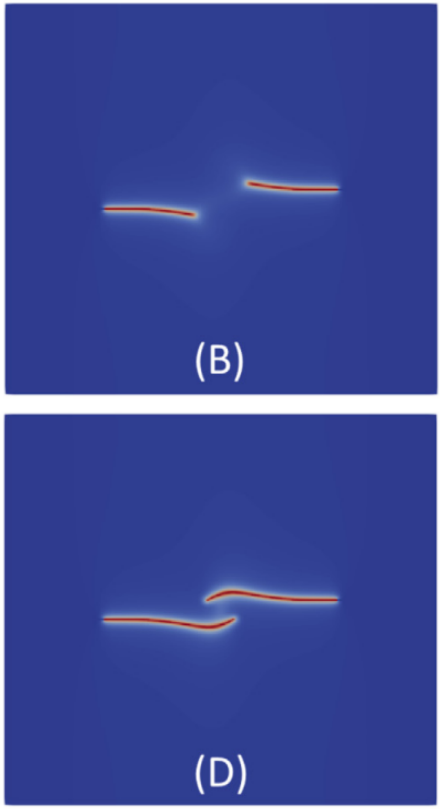

Zoom

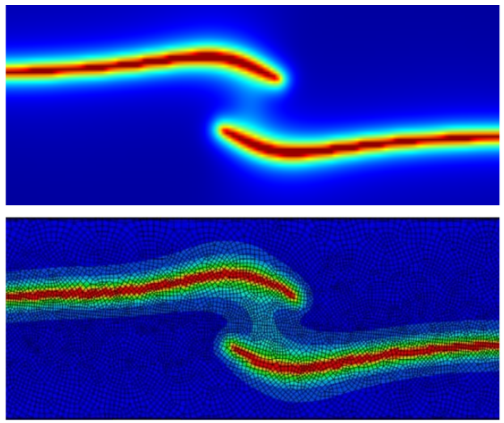

FE: Molnár et al, 2017

Contents

Performances

From Bary et al, 2011 (linear elasticity)

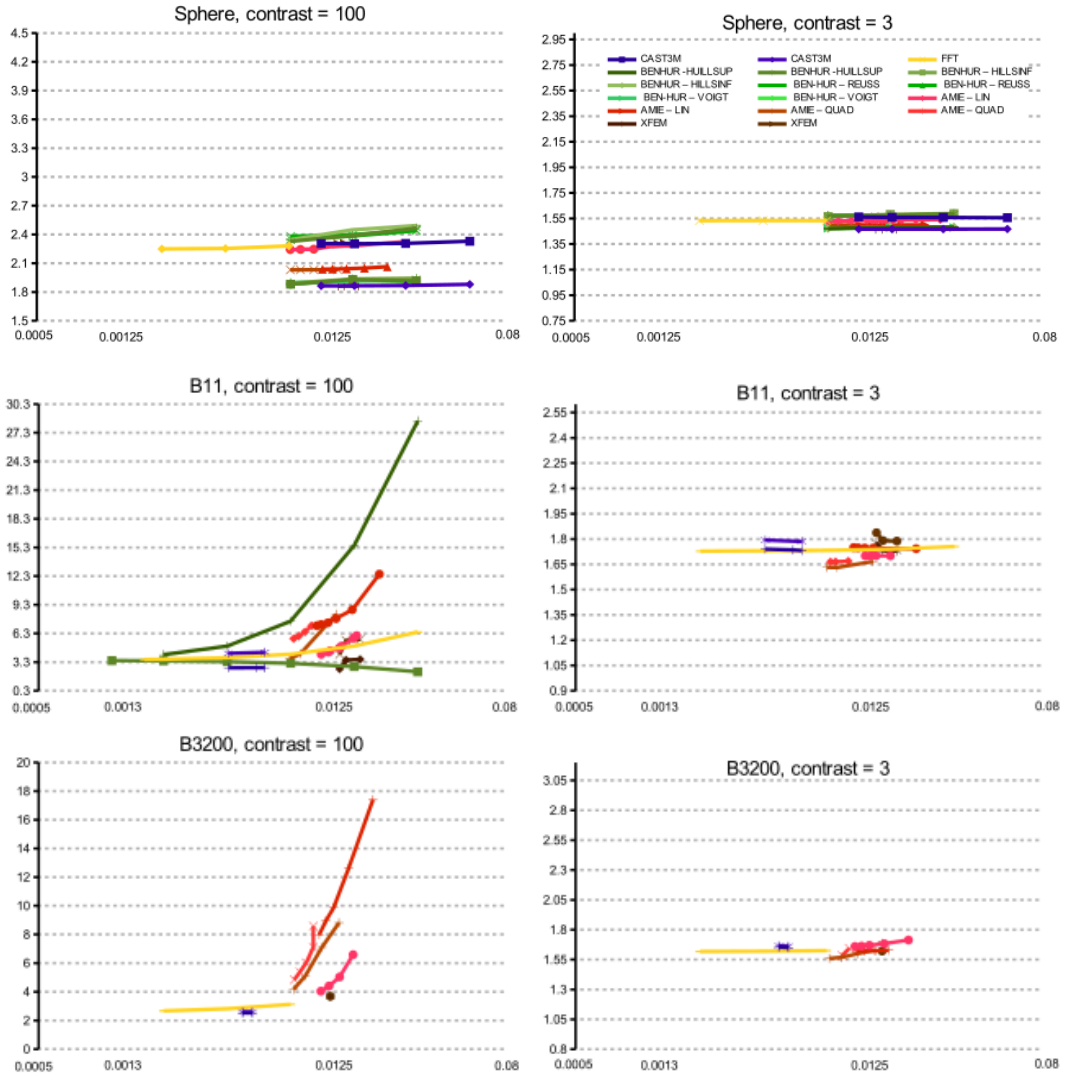

Performances and accuracy

Numerical optimization of microstructures properties with viscoelastic behavior (Koishi et al, 2017).
$4,000$ configurations of 1024^3 each on TSUBAME supercomputer at Global Scientific Information and Computing Center in Tokyo Institute of Technology though the HPCI System Research Project

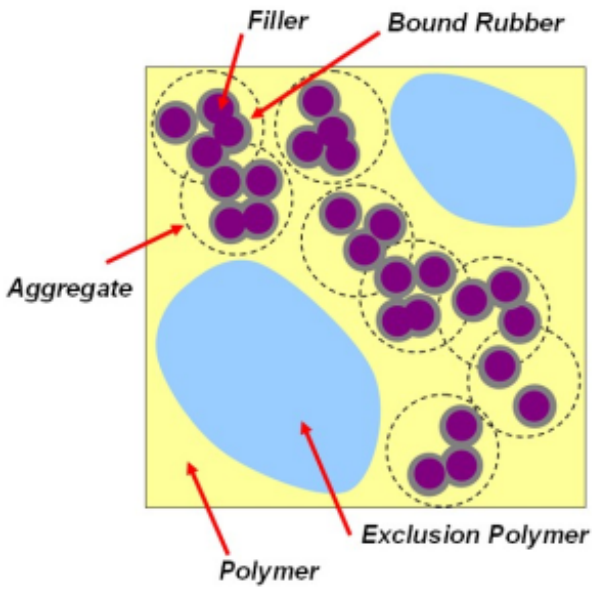

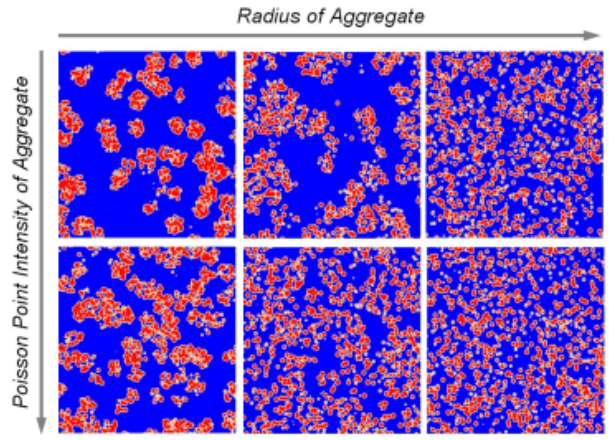

Figure 4. Cross section of six 3D simulation models generated with different Poisson point intensity and radius of aggregate, domain size: 1,000nm x 1,000nm x 1,000nm, the volume fraction of filler: 15%, the radius of filler: 10nm, the thickness of bound rubber: 5nm.

Performances and accuracy

From Koishi et al, 2017. Use of the rotated scheme with polarization method.

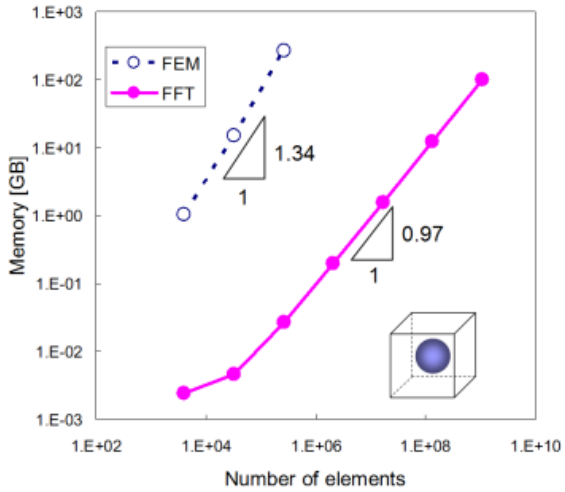

Figure 6. Required memory size of the FFT-based scheme and FEM against the number of elements.

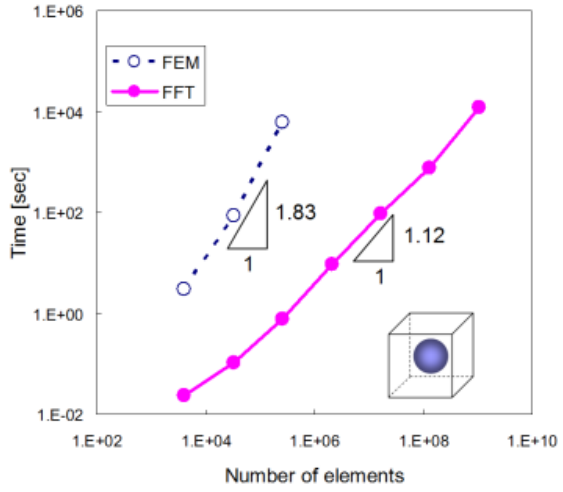

Figure 5. Computation time of the FFT-based scheme and FEM against the number of elements.

Performances and accuracy

Dealing with cracks.

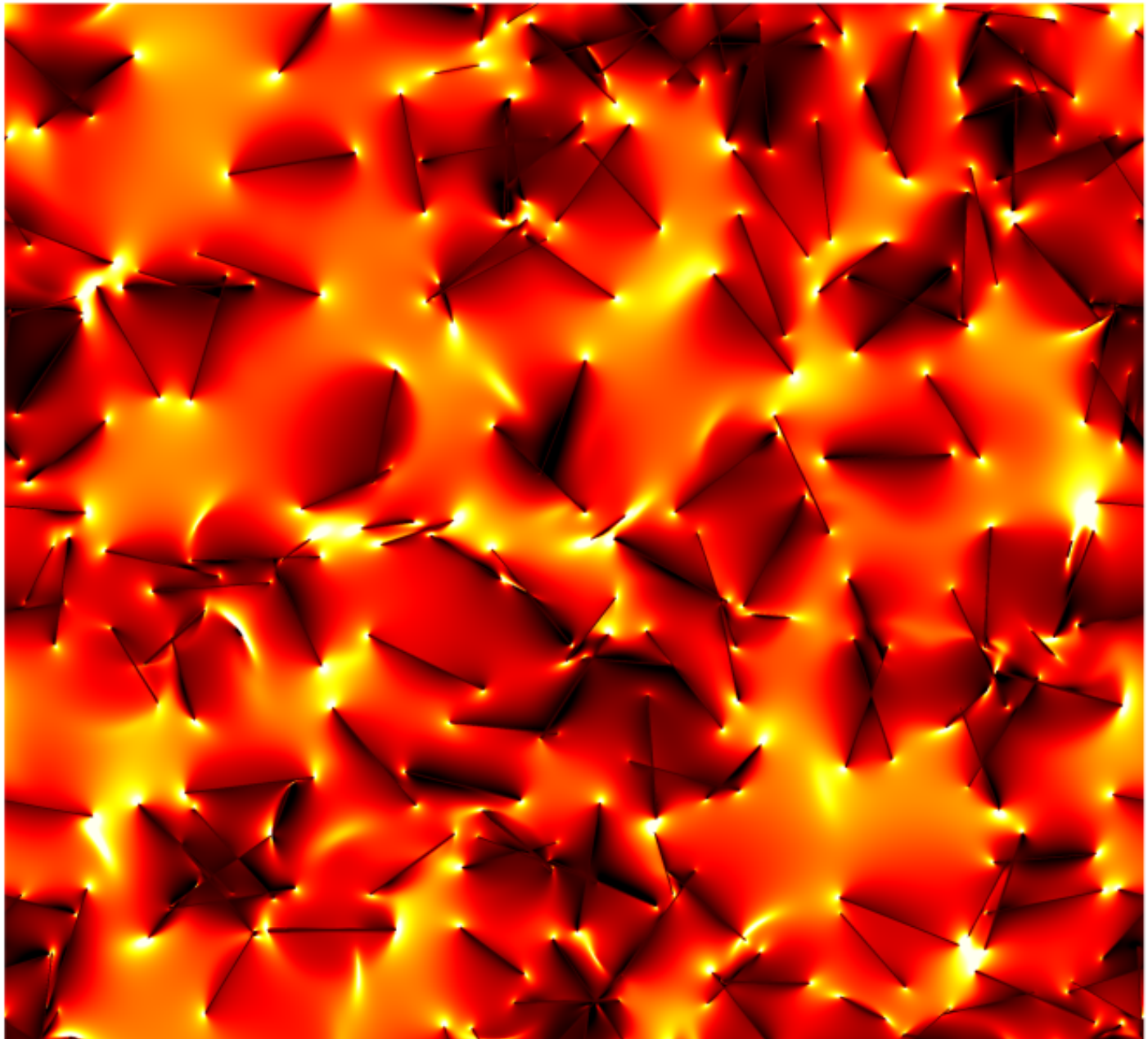

Performances and accuracy

From Gasnier et al (2018).

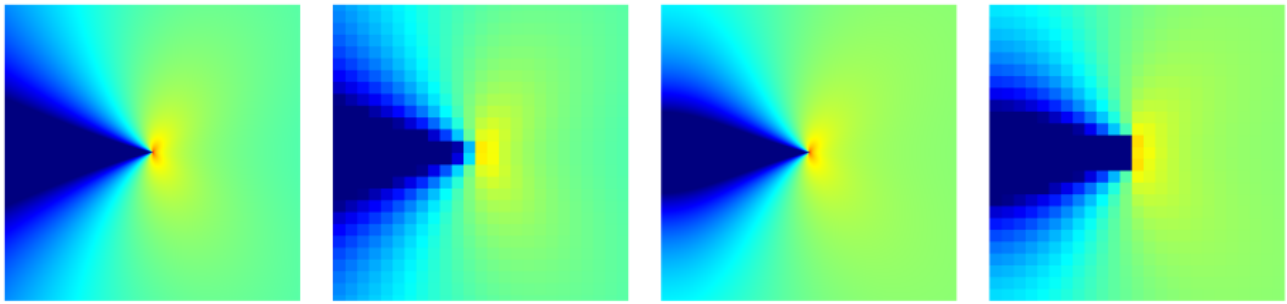

Figure 2: Stress component σ_{yy} in a region centered around an isolated crack tip, in a 2D medium. (a): Asymptotic expansion (5); (c-d): FFT predictions for the backward-and-forward scheme (FFT-BF) on grids of 4096^2 (c) and 128^2 voxels (d); (b): local averages of the asymptotic expansion (a) on the same coarse voxel-grid as used in (d). The same color map, ranging from blue (lowest value) to red (highest value) is used in maps (a-d).

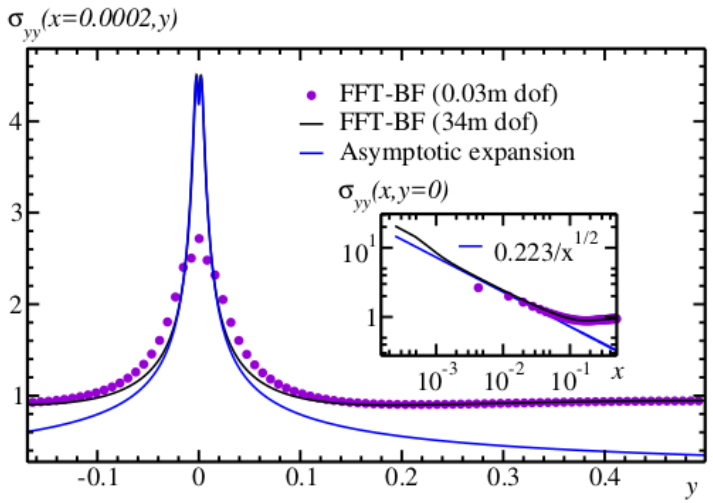

Figure 1: Periodic array of cracks in plane strain: profile of the stress component σ_{yy} along the segment $x = 2\,10^{-4}$, $-0.15 < y < 0.5$, close to the crack tip at $x = y = 0$. Solid black line and purple dots: Fourier backward-and-forward scheme with 34 millions and 32 thousands degrees of freedom. Solid blue line: asymptotic expansion near the crack tip (5) fitted with the value $K_I = 0.556$. Embedded graph (right): plot of σ_{yy} along the segment $y = 0$, $x > 0$, in log-log scale.

Performances and accuracy

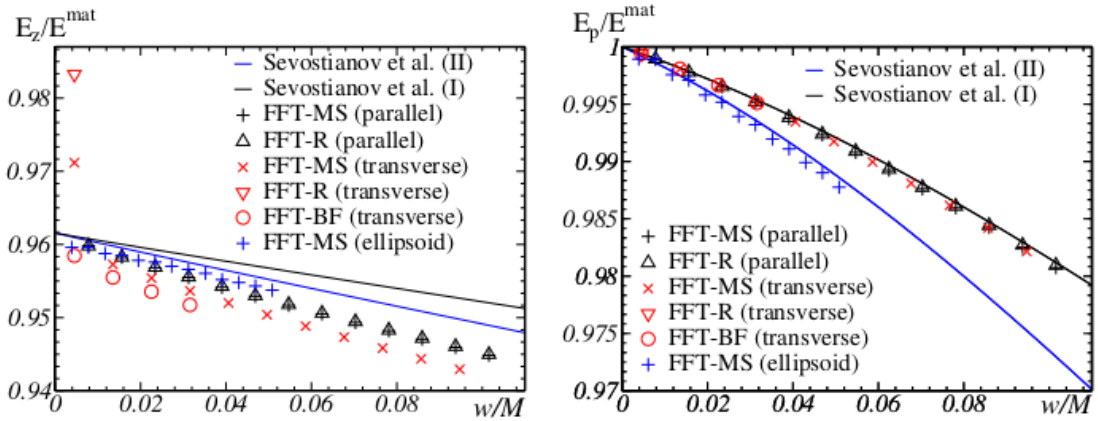

Figure 10: Influence of the crack's width w on the effective elastic moduli of a periodic array of cracks: Young moduli E_z and E_p. Symbols: FFT data points for cracks with cylindrical shape oriented parallel (black) and transverse (red) to the voxel grid and for ellipsoidal cracks with axis parallel to the voxel grid (blue). Solid lines: exact result for non-interacting parallel ellipsoidal voids. Black: with the same volume as the cylinders (method I). Blue: with lowest semi-axis $w/2$ (method II).

Cracks

From Gasnier et al (2018). Displacement field. Use of different discretizations.

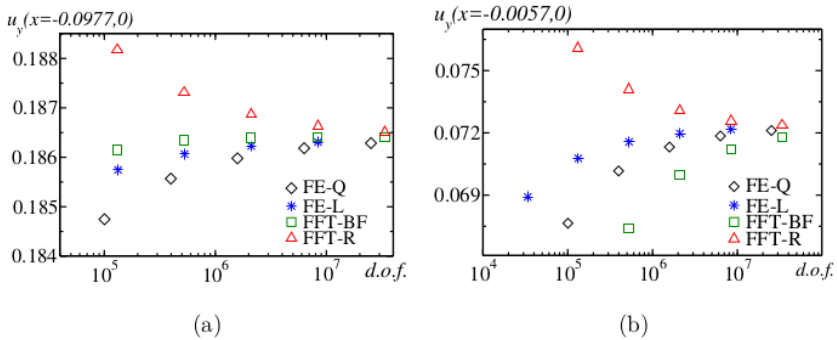

Figure 9: Continuation of Figs. 7 and 8: one value of the displacement component u_y in the middle of the crack ($y = 0$, $x = -0.977$) (a) and near the crack-tip ($y = 0$, $x = -0.0057$) (b), as a function of the number of degrees of freedom: finite element with linear elements (stars), quadratic elements (diamonds), Fourier methods with backward-forward (squares) and rotated (triangles) schemes.

Liu et al, (2020) report a 5 to 10% difference.

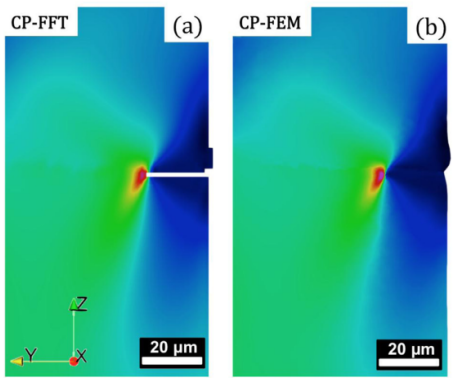

Fig. 6. The σ_{33} fields for (a) CP-FFT vs. (b) CP-FEM comparison for a zoomed view near the crack tip (displaying the dashed-box region shown in Fig. 5).

- Lucarini and Segurado (Computational Mechanics, 2019). Crystal plasticity with fatigue. Difference of the order of 7%. FFT is 6-7 times faster *and allows to compute models with sizes not accessible using FEM*.
- Vondrejc and de Geus (Journal of Computational and Applied Mathematics, 2020) : FEM more accurate than FFT when the material properties display jumps, mixed results obtained when the material properties vary smoothly.

Contents

Stokes flow

Incompressible Newtonian fluid with viscosity μ :

$$\begin{aligned} \mu\Delta \boldsymbol{u} &= \nabla \cdot P \qquad \text{(Stokes equation)} \\ \boldsymbol{u} &= 0 \qquad \text{(no-slip boundary condition at fluid-solid interface)} \\ \mathrm{div}\boldsymbol{u} &= 0 \qquad \text{(fluid incompressibility)} \end{aligned}$$

Periodic boundary conditions :

$$P(\boldsymbol{x}) = \boldsymbol{\alpha} \cdot \boldsymbol{x} + \phi(\boldsymbol{x}), \qquad \phi\#, \qquad \boldsymbol{u}\#$$

Loading : pressure drop $\boldsymbol{\alpha} = \langle \nabla \cdot P \rangle$

Permeability κ :

$$\mu\langle \boldsymbol{u} \rangle = \kappa \langle \nabla \cdot P \rangle = \kappa \cdot \boldsymbol{\alpha}$$

FFT methods for Stokes flow

Stokes equation equivalent to :

$$\boldsymbol{d}(\boldsymbol{x}) = (\mathrm{grad}\boldsymbol{u}(\boldsymbol{x}))_{\mathrm{sym}}, \qquad \boldsymbol{d}_m = 0,$$

$$\boldsymbol{\sigma}(\boldsymbol{x}) = 2\mu\boldsymbol{d}(\boldsymbol{x}) - P(\boldsymbol{x})\mathbf{I}, \qquad P(x) = \boldsymbol{\alpha}\cdot\boldsymbol{x} + \phi(\boldsymbol{x})$$

$$\mathrm{div}\boldsymbol{\sigma} = 0$$

Idea (Bignonnet and Dormieux, 2014) : extend the equations over the solid phase, treated as an incompressible viscuous fluid with infinite viscosity ($\mu = \infty$). No-slip boundary condtions automatically met, however rigid body motion of the solid domain must be prevented. If there is one connected component spaning the medium, it is sufficient to enforce $u = 0$ at one point in the solid phase or on average.
There must be body forces in the solid phase that counterbalance the macroscopic fluid pressure gradient.

$$\mu(\boldsymbol{x}) = \begin{cases} \infty & \text{solid} \\ \mu_f & \text{otherwise.} \end{cases} \qquad \mathrm{div}\boldsymbol{\sigma} = \begin{cases} -\boldsymbol{\alpha}/f_s & \text{solid} \\ 0 & \text{otherwise.} \end{cases}$$

FFT methods for Stokes flow

Introduce a reference viscosity μ^0 and recast the problem as :

$$\boldsymbol{\sigma}(\boldsymbol{q}) = -\mathbf{Y}^0(\boldsymbol{q}) \cdot \overline{f}(\boldsymbol{q}) - \Delta^0(\boldsymbol{q}) : [\boldsymbol{d}(\boldsymbol{q}) - \frac{1}{2\mu^0} : \boldsymbol{\sigma}(\boldsymbol{x})]$$

$$\boldsymbol{d}(\boldsymbol{\sigma}) = A(\boldsymbol{x})[\boldsymbol{\sigma}(\boldsymbol{x}) - P(\boldsymbol{x})\mathbf{I}], \qquad A(\boldsymbol{x}) = \frac{1}{2\mu}\chi_f(\boldsymbol{x}) + \frac{1}{2\mu_s}\chi_s(\boldsymbol{x})$$

$$\mathbf{Y}^0(\boldsymbol{q}) = \frac{i}{|q|^4}[(\delta_{ij}q_k + \delta_{ik}q_j + \delta_{jk}q_i)|q|^2 - 2q_iq_jq_k], \qquad f = \mathrm{div}(\alpha_k x_k)$$

Iterative scheme (Monchiet and Bonnet, 2009) :

$$\boldsymbol{\sigma}^{k+1}(\boldsymbol{q}) = \boldsymbol{\sigma}^k(\boldsymbol{q}) - \Delta^0(\boldsymbol{q}) : \mathbf{d}^k(\boldsymbol{q}), \qquad \boldsymbol{\sigma}^1(\boldsymbol{q}) \equiv -\mathbf{Y}^0(\boldsymbol{q}) \cdot \overline{f}(\boldsymbol{q})$$

Common choices : $\mu^0 = \mu_f$ or $\mu^0 = 2\mu_f$, $4\mu_f$ (in-between μ_f and ∞).

FFT methods for Stokes flow

Bignonnet and Dormieux : polarization scheme with variational framework. Introduce a reference viscosity μ^0 :

$$\boldsymbol{\tau}(\boldsymbol{x}) = \boldsymbol{\sigma}(\boldsymbol{x}) - 2\mu^0 \boldsymbol{d}(\boldsymbol{x})$$

Green function G^0, third-order Green operator $\mathcal{G}^0$, fourth-order Green operator Γ^0 :

$$\begin{aligned} \boldsymbol{u} &= \overline{\boldsymbol{u}} + G^0 * f_S^{-1} \chi^S \boldsymbol{\alpha} + \mathcal{G}^0 * \boldsymbol{\tau}, \\ \boldsymbol{d} &= -\Gamma^0 * \boldsymbol{\tau} +^t \mathcal{G}^0 * f_S^{-1} \chi^S \boldsymbol{\alpha}, \end{aligned}$$

with $\overline{\boldsymbol{u}} = -f_S^{-2} \overline{\chi^S G^0 * \chi^S} \cdot \boldsymbol{\alpha} = -G_0^{SS} \cdot \boldsymbol{\alpha}$

Tensors G^0, $\mathcal{G}^0$ and Γ^0 have simple forms in Fourier space (for the problem in the continuum).
In these methods, the solid phase must form one continuous phase.
Different discretizations (e.g. finite-differences) are possible. See Bignonnet (2020).

FFT methods for Stokes flow

Method developed by A. Wiegmann (2007). Velocity field evaluated at the center of the voxel faces, pressure field at the center of the voxels.

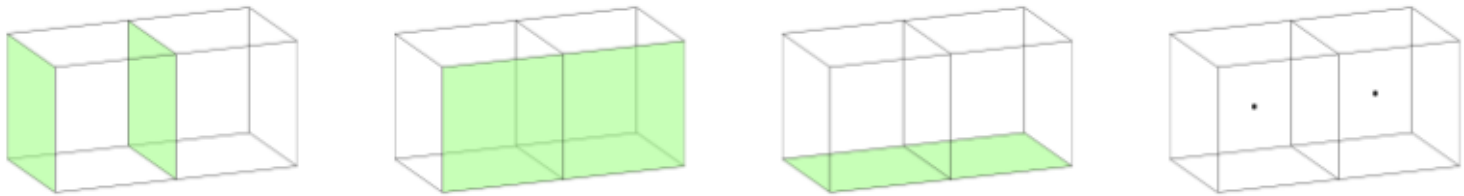

With local centered differences, $\Delta \boldsymbol{u}$ and $\nabla \cdot P$ evaluated at the center of voxel faces, and div$\boldsymbol{u}$ at the voxel centers.

$$\begin{aligned}
\Delta \boldsymbol{u}(\boldsymbol{x}) &\approx \Delta_h \boldsymbol{u}(\boldsymbol{x}) = \frac{\sum_i [\boldsymbol{u}(\boldsymbol{x}+e_i) + \boldsymbol{u}(\boldsymbol{x}-e_i) - 2\boldsymbol{u}(\boldsymbol{x})]}{h^2}, \\
(\partial_i P)(\boldsymbol{x}+e_i/2) &\approx (\nabla_h P)\cdot e_i = \frac{P(\boldsymbol{x}+e_i) - P(\boldsymbol{x})}{h}, \\
(\mathrm{div}\boldsymbol{u})(\boldsymbol{x}) &\approx (\mathrm{div}_h \boldsymbol{u})(\boldsymbol{x}) = \sum_i \frac{u_i(\boldsymbol{x}+e_i/2) - u_i(\boldsymbol{x}-e_i/2)}{h}
\end{aligned}$$

FFT methods for Stokes flow

No slip boundary conditions ?

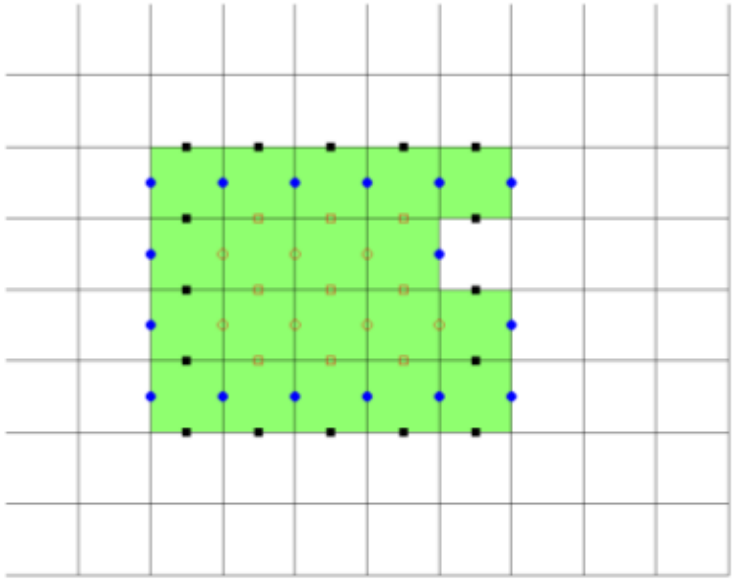

Method "FFF" : $\boldsymbol{u} = 0$ along blue and black points. Enforces normal and tangential no-slip boundary conditions.
Discretized system rewritten as

$$\mu \Delta_h u = \nabla_h P + \boldsymbol{f}$$

The force $\boldsymbol{f}$ takes non-zero values along the fluid-solid interface. Fields P and $\boldsymbol{u}$ can be computed from $\boldsymbol{f}$. System solved by conjugate gradient method. Popisson equation solved by FFTs (Wiegmann, 2007).

Results : 2D cylindrical obstacle

Velocity field (horizontal component). Exact solution obtained using the asymptotic expansion of Sangani & Acrivos (1981). FFF 100^2 voxels. Error $\times 20$.

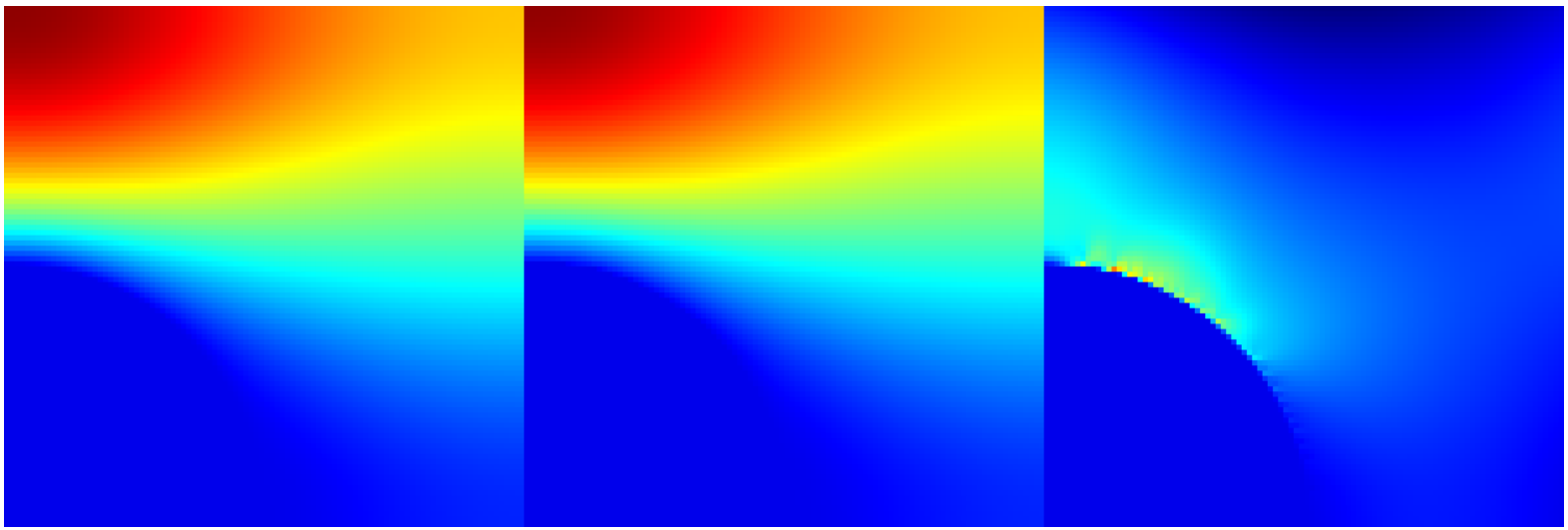

As expected, the error is maximum along the interface.

Results : 2D cylindrical obstacle

Fluid flow inside anode material used in fuel cells (Abdallah, 2016).

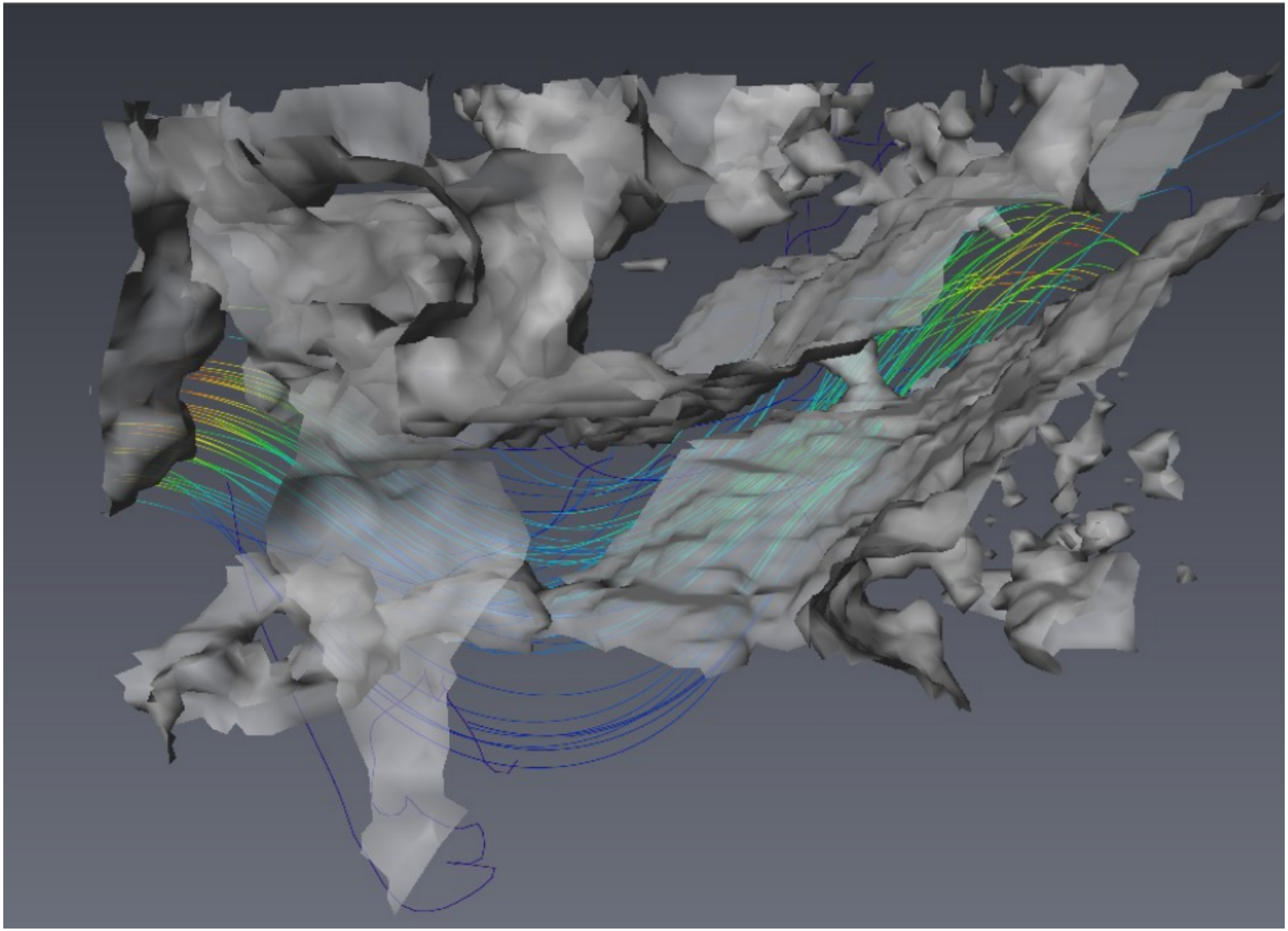

Contents

Topics not addressed here :

- Dislocations. Bertin, Capolungo, Berbenni, Suquet, Brenner.
- Strain gradients. Gélébart, Forest.
- Periodic boundary conditions.
- Finite strain. Lahellec (2003), Lebensohn (2013), Kabel (2014). Requires a different Green operator to take into account local rotations.